Supporting Information

Activation of low-cost stainless-steel electrodes for efficient and stable anion-exchange membrane water electrolysis

Tao Jiang [a]*, Leila Zouridi [b, c], Nannan Li [a], Vassilios Binas [c, d], Marc. C. A. Stuart [e], PV Aravind [f], Bayu Jayawardhana [a], Paolo P. Pescarmona [a], Vasileios Kyriakou [a]*

[a] *Engineering and Technology Institute Groningen (ENTEG), University of Groningen, Nijenborgh 4, 9747 AG, Groningen, The Netherlands*

[b] *Department of Materials Science and Technology, University of Crete, Heraklion, Greece*

[c] *Institute of Electronic Structure and Laser, Foundation for Research and Technology-Hellas, Greece*

[d] *Department of Chemistry, Aristotle University of Thessaloniki, Thessaloniki, 54124, Greece*

[e] *Groningen Biomolecular Sciences and Biotechnology institute, University of Groningen, Nijenborgh 7, 9747 AG Groningen, The Netherlands*

[f] *Energy and Sustainability Research Institute Groningen (ESRIG), University of Groningen, Nijenborgh 4, 9747 AG, Groningen, The Netherlands*

AUTHOR INFORMATION

Correspondence

Dr. T. Jiang: taojiang0510@gmail.com

Dr. Vasileios (Vassilis) Kyriakou: v.kyriakou@rug.nl

Experimental section

Materials and chemicals

304 type stainless steel mesh (80 mesh, Van Rooy & Co's Draadproducten B.V., Netherlands); Ni mesh (80 mesh, Alfa Aesar); 0.1 M H_2SO_4 solution (Sigma-Aldrich®); $Na_2SO_4 \cdot 10H_2O$ (≥ 99.0%, Sigma-Aldrich®); $FeCl_3 \cdot 6H_2O$ (≥ 98.0%, Sigma-Aldrich®); KOH (90.0%, Sigma-Aldrich®); Nafion (Alfa Aesar); 5 cm² AEM cell hardware (Dioxide materials); Sustainion® X37-50 Grade 60 Membrane (Dioxide materials).

Preparation of the SM-CA pre-catalysts.

A modified etching method[1] was employed to process the steel mesh (SM), which helped create a suitable surface morphology and remove any impurities that could hinder electrocatalytic activity. The SM (35×35×0.5 mm³) was ultrasonically cleaned by 0.1 M H_2SO_4 solution, acetone, DI water, and absolute ethyl alcohol in sequence, and then dried in the air for 1 min. Firstly, 0.02 mol of $FeCl_3 \cdot 6H_2O$ (iron chloride hexahydrate) and 0.002 mol of $Na_2S_2O_3 \cdot 10\,H_2O$ (sodium thiosulfate pentahydrate) were dissolved in separate beakers, each with an appropriate volume of DI water. The solutions were then transferred, one after the other, into a third beaker. DI Water was added to reach a final volume of 100 ml. The mixed solution was observed, and the color changed from dark purple to brownish yellow, indicating the desired solution formation. Two pieces of SM samples were dipped several times in the solution and then they were immersed in the beaker at a depth of 30 mm. The beaker, containing the SM samples, was placed in a 50°C water bath and subjected to magnetic stirring for 5 minutes. After the activation process, the obtained SM-CA samples were carefully removed from the solution and sequentially rinsed with water and absolute ethyl alcohol to remove any residual solution and impurities. These activated SM-CA pre-catalysts were then prepared for subsequent electrochemical activation.

Preparation of SM-CA-H and SM-CA-O electrodes

The second step involved an ion exchange strategy through a simple electrochemical activation, which allowed for the introduction of desired catalytic species onto the surface of the stainless steel meshes. Electrochemical activation of the prepared SM-CA (35×35×0.5 mm³) pre-catalysts was simply implemented by employing 2 pieces of SM-CA samples as both cathode and anode under 200 mA cm⁻² (1 M KOH at RT) driven by a power supply (VOLTCRAFT DSP-6010) for 20 min and 2 hours. The resulting cathode and anode were identified as SM-CA-H and SM-CA-O, respectively, which would be evaluated in a three-electrode-test system and constructed in a 5 cm² AEM electrolyzer cell.

Fabrication of Pt/C@SM electrodes

To prepare the Pt/C@SM electrodes, 100 mg Pt/C (Alfa Aesar), 200 μL Nafion (Alfa Aesar), 1 mL ethanol, and 1 mL deionized water were ultrasonicated for 60 min to obtain a homogeneous dispersion. Then, a piece of clean SM (30×30×1 mm³) was dipped into the dispersion, then dried in air at 333 K for 6 h. The mass loading of the Pt/C catalyst on SM was controlled to be ca. 3.5 mg cm⁻², as determined by weighing the sample prior to and following the treatment.

Fabrication of IrO₂@SM electrodes

To prepare the IrO₂@SM electrodes, 100 mg IrO₂ (Alfa Aesar), 200 μL Nafion (Alfa Aesar), 1

mL ethanol, and 1 mL deionized water were ultrasonicated for 60 min to obtain a homogeneous dispersion. Then, a piece of clean SM ($30 \times 30 \times 1$ mm^3) was dipped into the dispersion, which was then dried in air at 333 K for 6 h. The mass loading of the IrO$_2$ catalyst on SM was controlled to be ca. 4 mg cm^{-2}, as determined by weighing the sample prior and following the treatment.

Materials characterization

XRD data were collected using a Bruker D8 Advance diffractometer operating in Bragg-Brentano geometry with Cu Kα radiation (wavelength: 1.5418 Å). The 2θ scans were performed from 20° to 80° with a step size of 0.02° and a counting time of 1.00 s per step. Scanning electron microscopy images were obtained using a JEOL JSM-7000 SEM Microscope (JEOL Ltd., Tokyo, Japan) equipped with an EDX detector for elemental analysis and mapping. SPECS FlexMod XPS equipped with a 1D-DLD upgraded detector and an XR-50 Dual Anode X-ray source. The samples were attached to the sample holder with double-sided carbon tape. Data acquisition at a pressure lower than 1×10^{-6} Pa using a charge neutralization system. High-resolution transmission electron microscopy (HR-TEM) images of the catalysts were obtained using a Tecnai T20 electron microscope (FEI) operated at an accelerating voltage of 200 keV. The catalysts were dispersed in ethanol under ultrasonication and deposited on a holey carbon-coated copper grid (Quantifoil 1.2/1.3) for measurement. Fast Fourier transforms of high-resolution images were used to check for loss of ordering of the used H-ZSM-5 crystals. Energy Dispersive X-ray (EDX) analyses were performed on an X-Max T80 SDD detector (Oxford instruments) and were combined with high-angle annular dark field STEM images for both elemental composition and location. In general, 4-10 spots of each sample were analyzed and EDX mapping of three representative sites was presented (SI) Distilled water and ethanol were used to thoroughly clean all the samples before testing commenced. The contact angle measurement was carried out by dropping 6 µL deionized water on the electrode surface with a dosing rate of 1 µL s^{-1} (DataPhysics Optical Contact Angle System OCA 15EC) and the data were analyzed with the SCA20 software. The house-made camera equipment was used to record the bubble release behavior.

Electrochemical half-cell measurements (three-electrode test system)

All electrochemical measurements were carried out using an 8-channel IVIUM-n-Stat Electrochemical Workstation (Module 5A/5V-1 MHz) with a developed in-house three-electrode H-cell test bench. Hydrogen Reference Electrode HydroFlex (Gaskatel GmbH, Germany) was used as the reference electrode. The potential measured using this Hydrogen Reference Electrode (HRE) as the reference electrode did not require any complex conversion to Reversible Hydrogen Electrode (RHE), allowing any tested temperature and pH of the electrolyte, namely $E_{RHE} = E_{HRE}$. Furthermore, HRE is suitable for the full pH range from -2 to 16 and a temperature range from -30 °C to 200 °C. The cathode and anode electrode clips are aligned in parallel, with one end connected to the workstation wire. The opposite end securely holds both the counter electrode and the working electrode. The height is carefully adjusted to guarantee that a geometric area of 1 cm^2 (each side) is fully immersed in the electrolyte solution. To keep consistency with the other mesh electrode literature, both sides of the mesh are exposed to the electrolytes.[1, 2]

A nickel plate (10 mm$\times$10 mm$\times$0.5 mm) was used as the counter electrode (CE). SM-CA-H

was used directly as the working electrode in the HER test with bare SM (steel mesh), NM (nickel mesh), and Pt/C@SM as control samples. SM-CA-O was used directly as the working electrode in the OER test with bare SM, NM, and IrO$_2$@SM as control samples. To better illustrate the catalytic activity of the materials, we tested all the samples under 1 M KOH at RT. This study's current density values of LSV curves refer to the geometric surface area. 1 M KOH solutions were saturated with O$_2$ before OER tests at room temperature. Linear sweep voltammogram (LSV) curves were recorded at a scan rate of 3 mV s^{-1}, and each measurement was repeated at least three times to avoid any incidental error. To provide reliable electrochemical data and avoid the overlap between Ni^{2+}/Ni^{3+} oxidation and OER, polarization curves were recorded from high initial potentials to low final potentials.[3, 4] Tafel slopes were derived from LSV obtained by plotting overpotential against log (j, current density) after iR correction ($E_{iR}=E - j \times R_s$) in all the above test conditions.[5, 6] The electrochemical impedance spectroscopy (EIS) measurement was conducted in the frequency range of 100 kHz to 0.1 Hz with an amplitude of 5 mV under a fixed bias of–0.4 V vs. RHE (η = 400 mV) for HER, and 1.53 V vs. RHE (η = 300 mV) for OER.

The double-layer capacitance (C$_{dl}$) was determined by measuring the capacitive current associated with double-layer charging from the scan-rate dependence of CVs. For this, the potential window for CVs was 0.2-0.4 V vs. RHE for HER and 1.07-1.17 V vs. RHE for OER. The scan rates were 10,20, 40, 60,80, and 100 mV s^{-1}. The C$_{dl}$ was estimated by plotting the $\Delta J = (J_a - J_C)$ at 0.3 V (HER) and 1.12 V (OER) vs. RHE against the scan rate. The linear slope is twice the C$_{dl}$.

5 cm^2 AEM electrolyzer cell measurements

A commercial AEM electrolyzer cell driven by an 8-channel IVIUM-n-Stat Electrochemical Workstation (Module 10A/5V-1 MHz) was employed to examine the performance of the prepared electrodes. Square-shaped 5 cm^2 SM-CA-H and SM-CA-O as the cathode and anode were assembled horizontally with Sustainion® X37-50 Grade 60 Membrane as a separator in the commercial AEM electrolyzer cell. Gaskets are made of PTFE, with squared 5 cm^2 openings. The cell is made of nickel plates, with channels through which the electrolyte flows on the inner side of the nickel plates, which also serve as the current collectors on each side of the cell. The schematic component of the AEMWE is shown in Figure S16. 8 stainless steel fastening bolts are used to secure the final assembly of the electrolyzer. A Digital Torque Screwdriver was used to control the torque applied to the cell. The cells were operated vertically, and 1 M KOH electrolytes were pumped into the cell with a flow rate of 300 ml min^{-1}. After 30 min of activation at a constant current of 0.5 A, the cells were characterized by recording I-U curves with a scan rate of 3 mV s^{-1} and the max current up to 10A. As references, the other two cells with bare SM and NM as both the anode and cathode sides with Sustainion® X37-50 Grade 60 Membrane as a separator were also tested under the same conditions. When reporting the current density, this was calculated based on the geometric area of one of the two sides of the mesh (the one facing the channels where the electrolyte flows), and thus not considering the contribution of the Ni plate to the activity. This was done for the sake of simplicity and following a common practice in the literature.[7-9] Since the cell configuration is the same in all tests, the calculated current densities allow meaningful comparison of the performance of the different meshes. Electrochemical Impedance Spectroscopy (EIS) was performed in galvanostatic mode with an 8-channel IVIUM-n-Stat Electrochemical

Workstation (Module 5A/5V-1 MHz) in a frequency range from 100 kHz to 0.1 Hz. To analyze the EIS plots, the fitting procedure was performed using the equivalent circuit chosen based on the physical processes and their interactions in the system, which include ohmic, cathodic charge transfer (HER), anodic charge transfer (OER), and mass-transfer resistances. The fitting of the Nyquist plot was done by the commercial Ivium software.
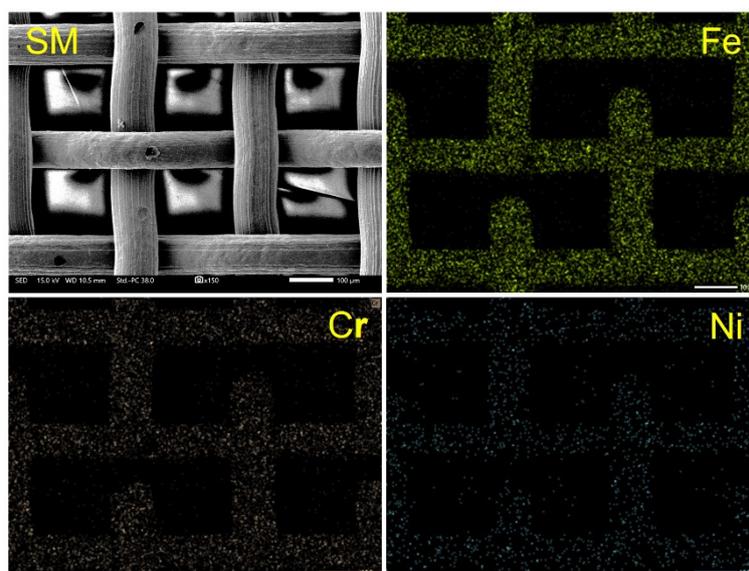

Figure S1. SEM image of the SM sample and the corresponding elements-mapping: Fe, Cr, and Ni.
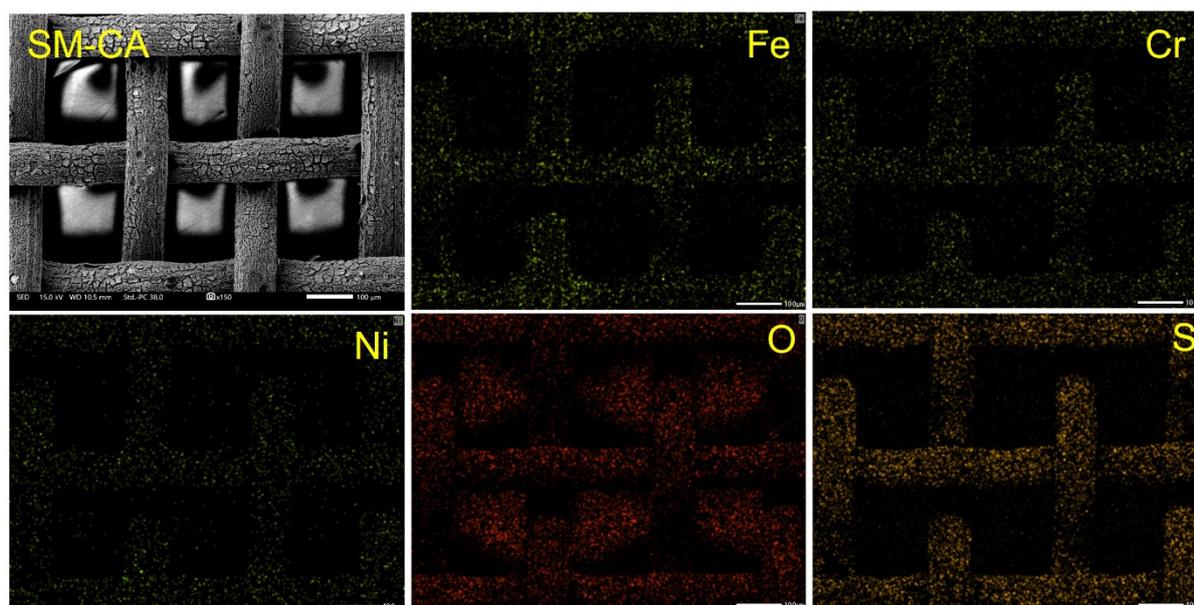
Figure S2. SEM image of the SM-CA sample and the corresponding elements-mapping: Fe, Cr, Ni, O, and S.

Table S1. SEM-EDS element contents of SM and SM-CA samples.

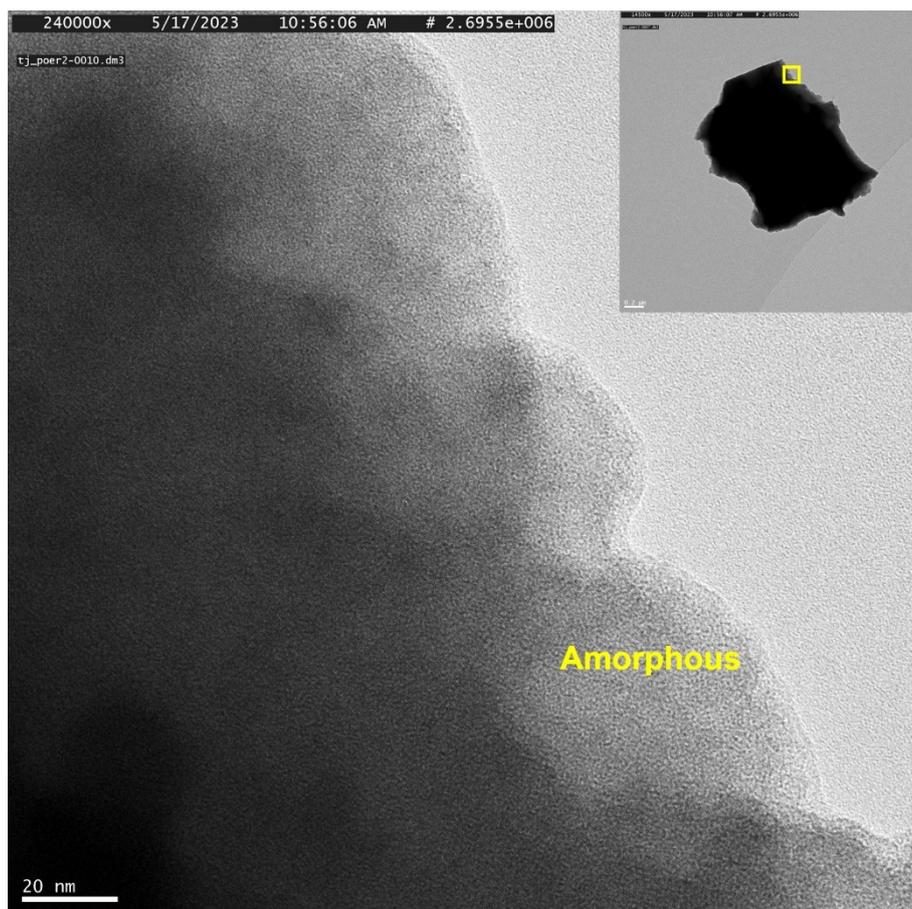| Samples	Fe/atom%	Ni/atom%	Cr/atom%	O/atom%	S/atom%
SM	69.6	11.3	19.1	0	0
SM-CA	10.3	6.6	9.2	58.5	14.4

Figure S3.TEM image of the SM-CA pre-catalyst, inset: low-resolution TEM image of flake exfoliated from the surface of SM-CA sample.
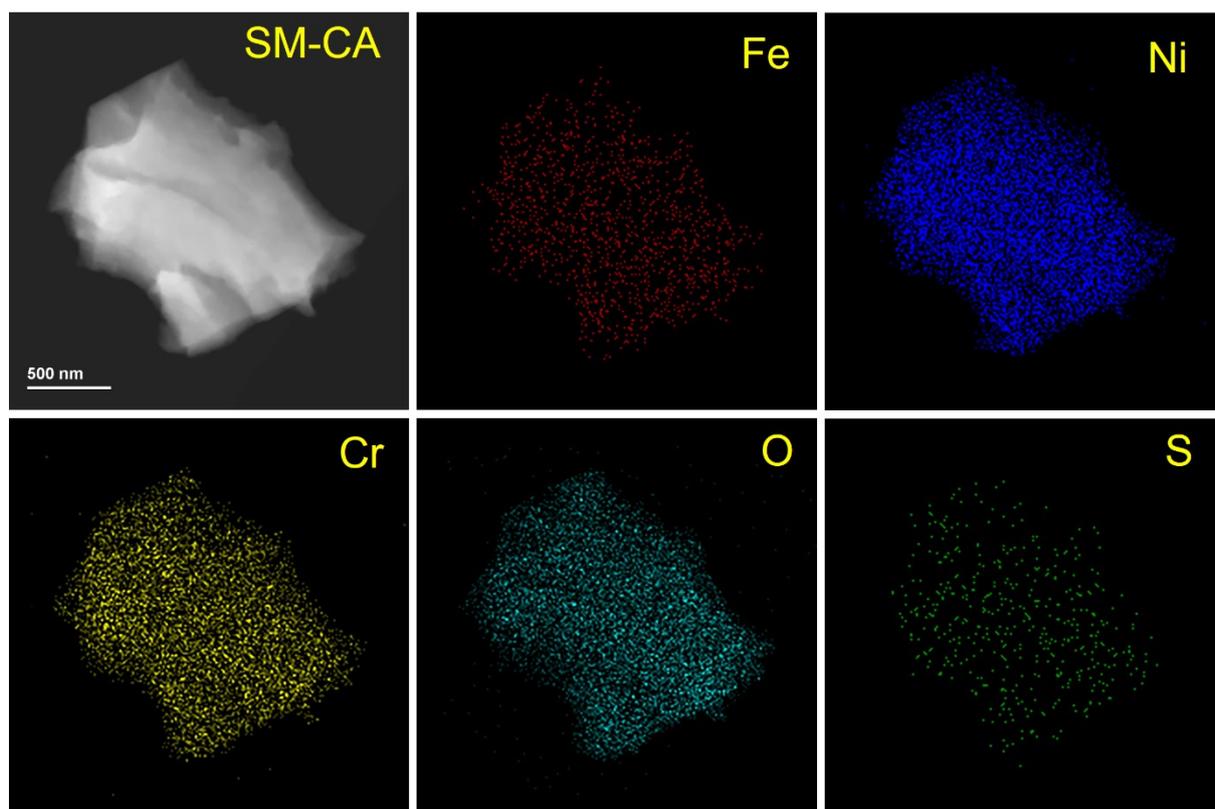
Figure S4. HAADF-STEM image of the SM-CA sample and the corresponding elements-mapping: Fe, Ni, Cr, O, and S.
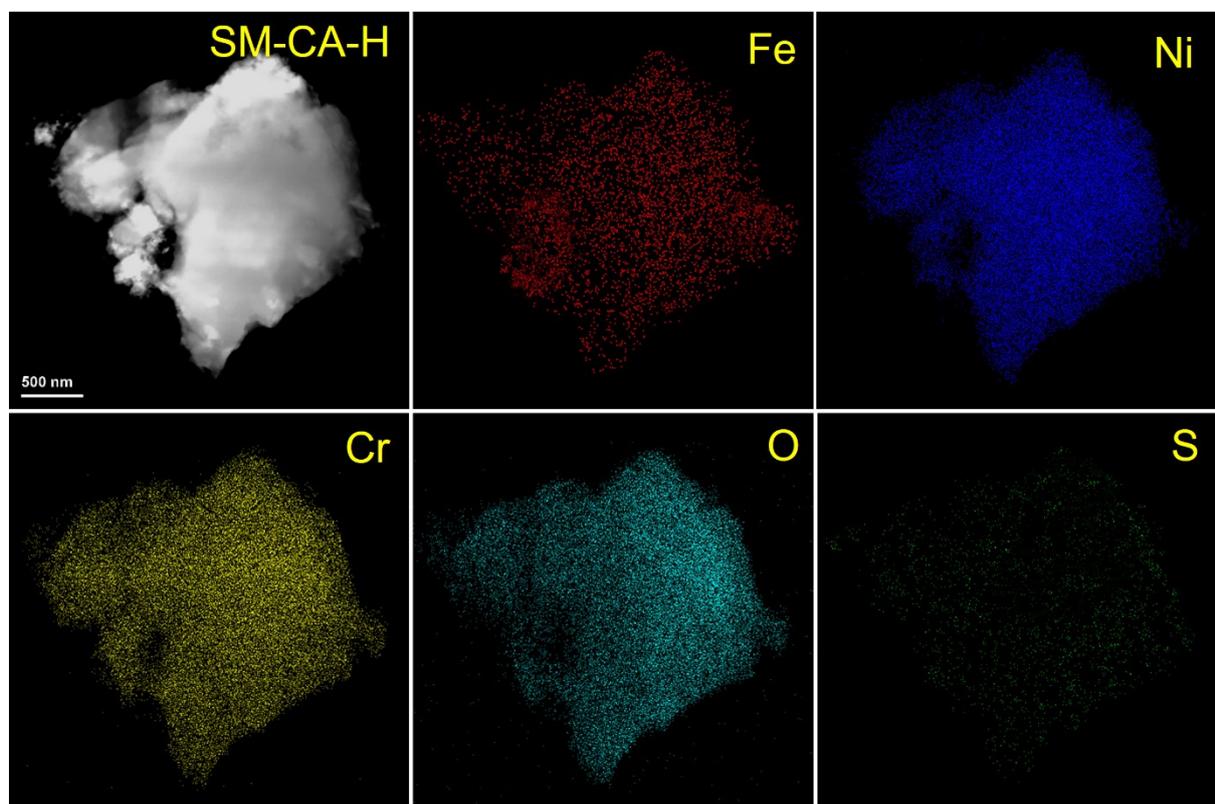

Figure S5. HAADF-STEM image of the SM-CA-H sample and the corresponding elements-mapping: Fe, Ni, Cr, O, and S.
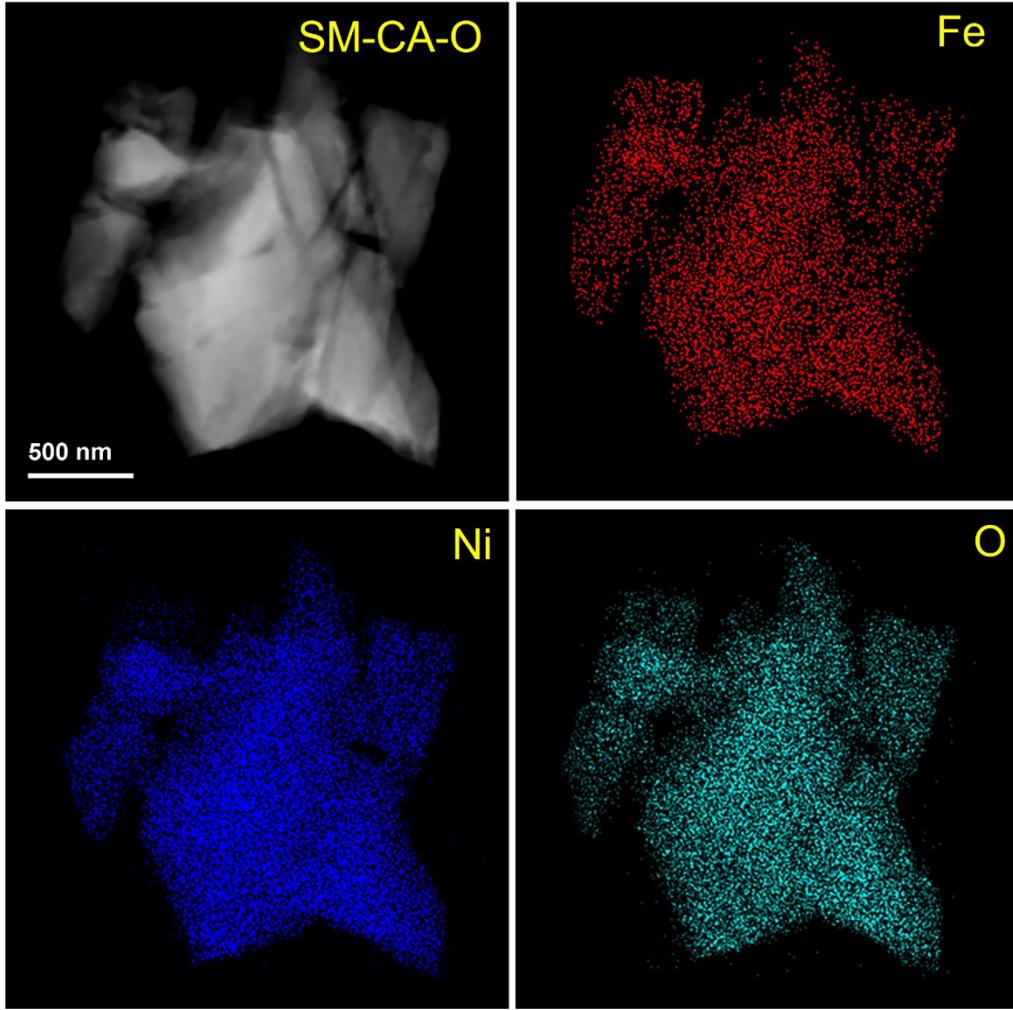
Figure S6. HAADF-STEM image of the SM-CA-O sample and the corresponding elements-mapping: Fe, Ni, and O.

Table S2. HAADF-STEM-EDS element contents of SM-CA, SM-CA-H, and SM-CA samples.

Samples	Fe/atom%	Ni/atom%	Cr/atom%	O/atom%	S/atom%
SM-CA	1.5	13.0	17.2	65.0	3.3
SM-CA-H	6.4	16.1	27.0	50.1	0.4
SM-CA-O	9.1	18.3	0	72.6	0

Table S3. The fitted equivalent circuit data (HER) of the employing samples.

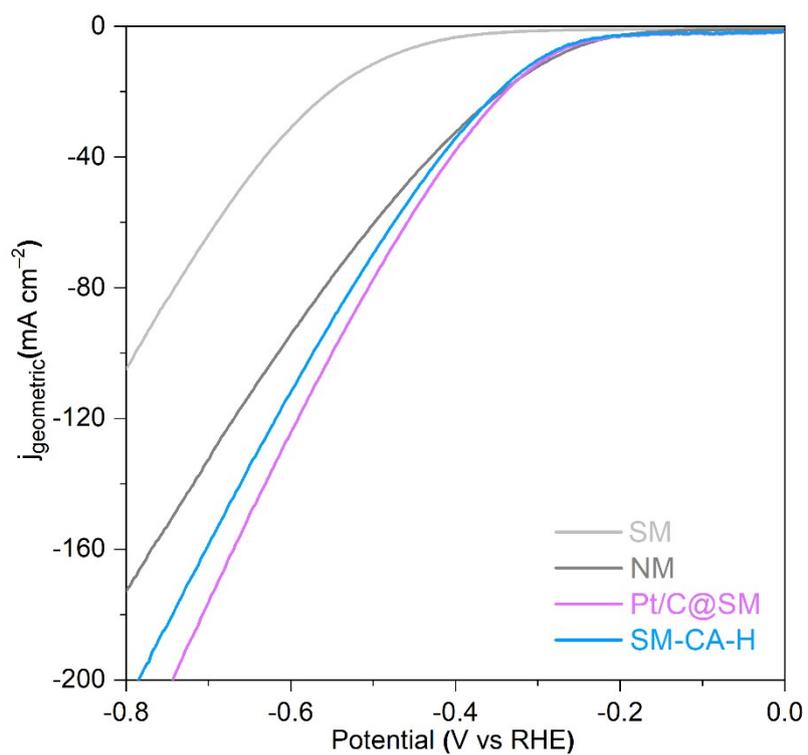| Samples	$R_s/\Omega\ cm^2$	$R_{ct}/\Omega\ cm^2$	CPE-T/S•s^(CPE-P)•cm^(−2)	CPE-P
SM	1.32	23.52	2.52×10^{-2}	0.89
NM	1.35	6.75	2.13×10^{-2}	0.90
SM-CA-H	1.38	3.98	1.14×10^{-2}	0.93
Pt/C	1.37	2.51	2.48×10^{-2}	0.91

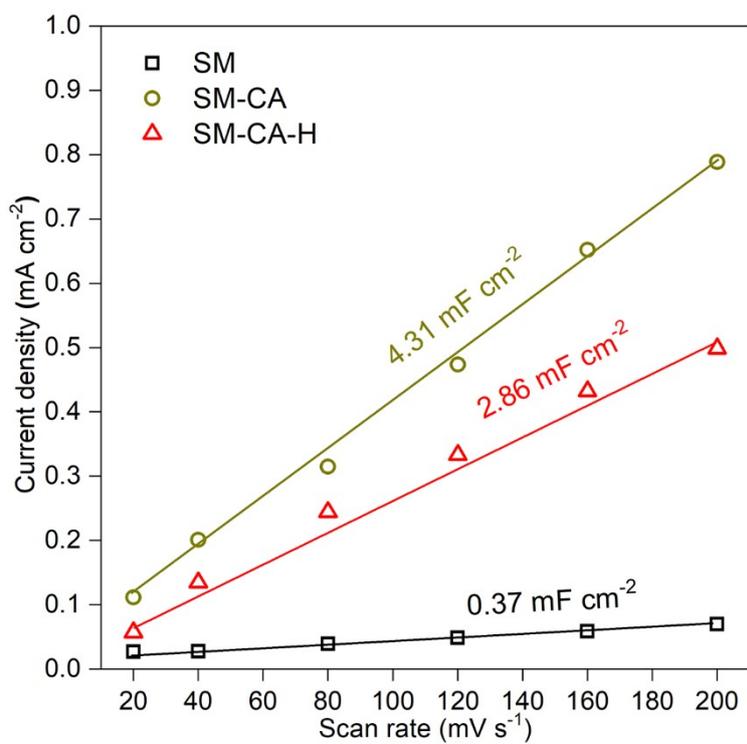Figure S7. LSV curves without iR-corrections of SM, SM-CA, and SM-CA-H towards HER.

Figure S8. C_{dl} curves of SM, SM-CA, and SM-CA-H towards HER.

Table S4. The HER activity of the prepared catalysts compared with state-of-the-art HER catalysts reported.

| Materials	Electrolyte	η_{10}, mV	Tafel slope, mV/dec
This work (SM-CA-H)	**1 M KOH**	**250**	**109**
This work (Pt/C-SM)	**1 M KOH**	**250**	**107**
316 Steel-OESSC [5]	1 M KOH	268	-
NiFeS@Ti$_3$C$_2$ MXene/NF [10]	1 M KOH	150	177
Ni@C-N-AG [11]	1 M KOH	150	68
NCS-P [12]	1 M KOH	77	68.5
NiCoMnFe-P2 [13]	1 M KOH	200	104
Ni/NiFe$_2$O$_4$@PPy [14]	1 M KOH	127	97
Mo$_2$NiB$_2$ [15]	1 M KOH	160	71
NiFeCoS$_x$@FeNi$_3$ [16]	1 M KOH	88	116
V-Ni$_3$FeN/Ni@N-GTs [17]	1 M KOH	66	88
m-NiTPyP/CNTs [18]	1 M KOH	138	83
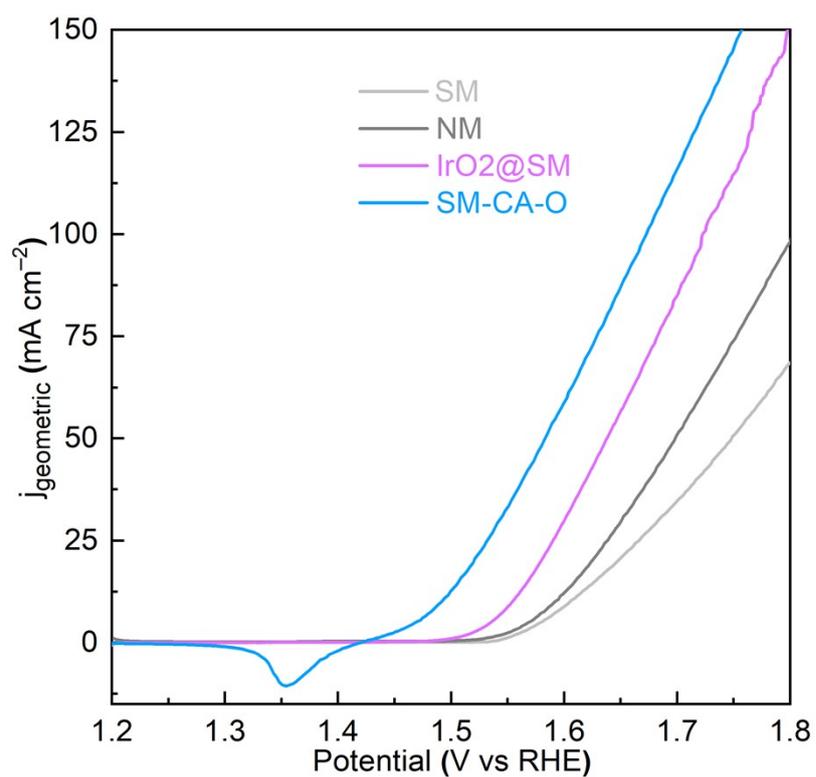
Figure S9. LSV curves without iR-corrections of SM, SM-CA, and SM-CA-H towards OER.

Table S5. The fitted equivalent circuit data (OER) of the employing samples.

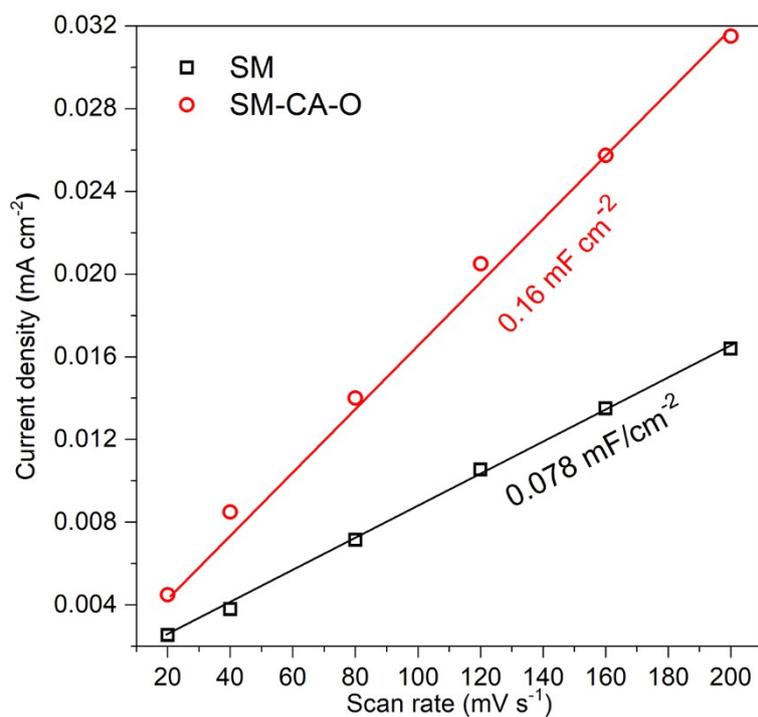| Samples	R_s / Ω cm^2	R_{ct} / Ω cm^2	CPE-T/S•s^(CPE-P)•cm^(−2)	CPE-P
SM	1.60	8.25	3.01×10^{-2}	0.88
NM	1.60	4.18	2.11×10^{-2}	0.90
SM-CA-O	1.62	0.91	1.10×10^{-2}	0.91
IrO$_2$@SM	1.64	2.02	2.58×10^{-2}	0.89

Figure S10. C_{dl} curves of SM, and SM-CA-O towards OER.

Table S6. The OER activity of the prepared catalysts compared with state-of-the-art OER catalysts reported.

Materials	Electrolyte	η_{10}, mV	Tafel slope, mV/dec
This work (SM-CA-O)	**1 M KOH**	**240**	**27**
This work (IrO$_2$@SM)	**1 M KOH**	**300**	**39**
NiS-450 [19]	1 M KOH	172	65
NiFeS@Ti$_3$C$_2$ MXene/NF [10]	1 M KOH	270	45
Ni@C-N-AG [11]	1 M KOH	290	93
NCS-P [12]	1 M KOH	273	42.2
NiCoMnFe [13]	1 M KOH	286	53
Ni$_2$Si PMEC [20]	1 M KOH	273	72.4
Ni/NiFe$_2$O$_4$@PPy [14]	1 M KOH	265	99
Ni-Co-Fe-P NBs [21]	1 M KOH	187	29

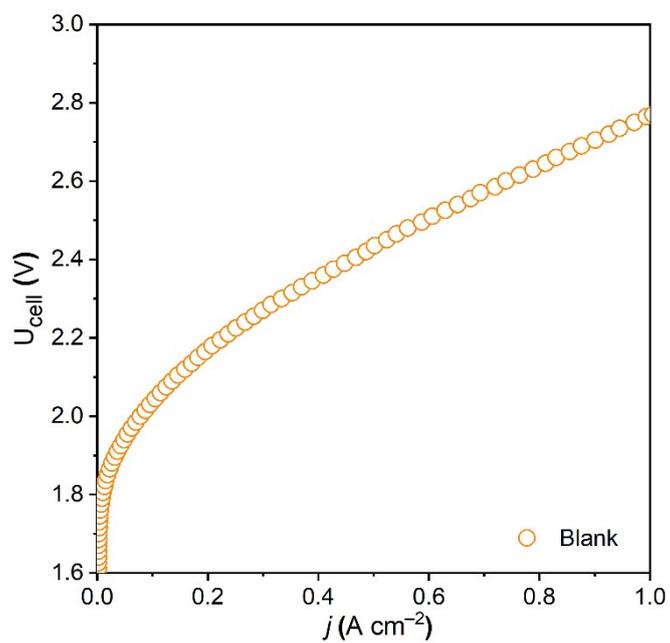|			
Ni$_{SA}$Fe$_{SA}$Ni$_{50}$Fe/CNT [22]	1 M KOH	227	41.8
NM@cNF/aNFO [23]	1 M KOH	100	19
Mo$_2$NiB$_2$ [15]	1 M KOH	280	57
NiFeCoS$_x$@FeNi$_3$ [16]	1 M KOH	210	45
V-Ni$_3$FeN/Ni@N-GTs [17]	1 M KOH	252	29
NiFeMOFs [24]	1 M KOH	258	49
Ni (S-Fe-Ni) [25]	1 M KOH	200	31.4
m-NiTPyP/CNTs [18]	1 M KOH	267	33.1
Ni$_3$N/Ru/NCAC [26]	0.1 M KOH	288	60

Figure S11. Background performance: AEM electrolyzer cell without electrodes. The effective area of the cell without electrode assembly is normalized by the 5 cm^2 channel area on the surface of the Nickel Bipolar Plate.
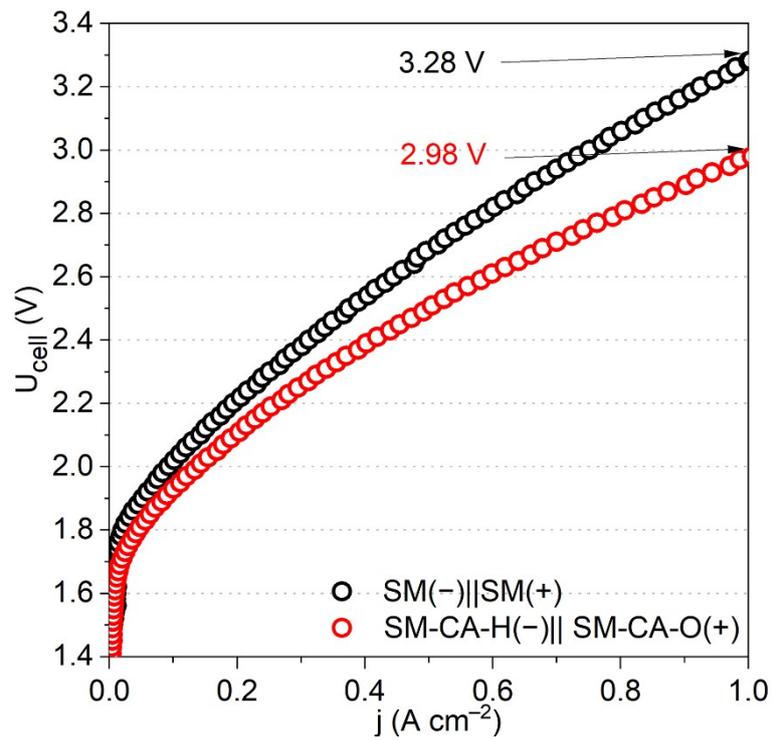
Figure S12. Polarization curves for different alkaline electrolyzer cells (Zirfon PERL as electrode separator): SM(−)‖SM(+) and SM-CA-H(−)‖SM-CA-O(+).
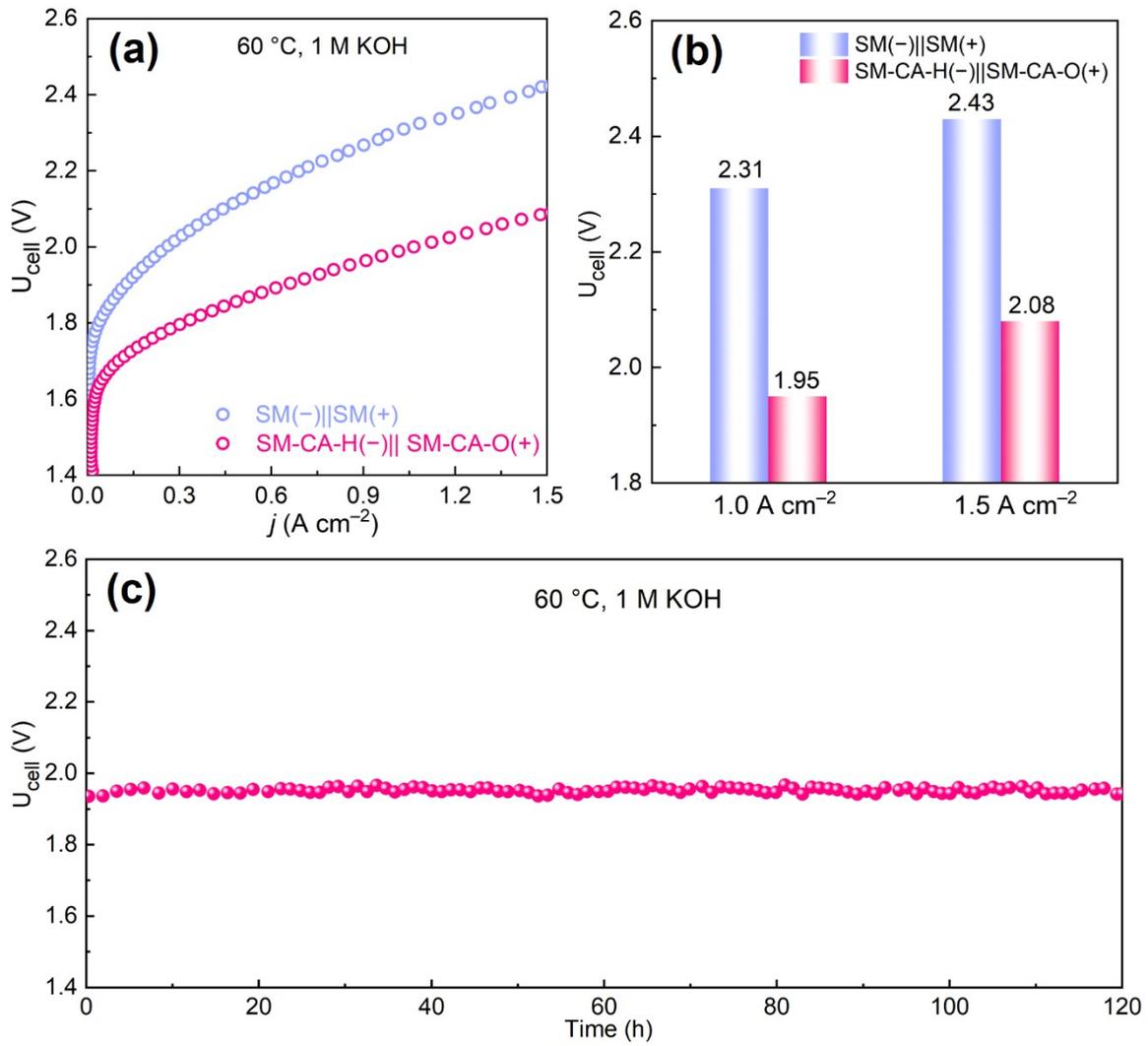
Figure S13. Impact of SM-CA-H(–)||SM-CA-O(+) on the performance of AEM electrolyzer cell (5 cm²). (a) Polarization curves for different cells: SM(–)||SM(+) and SM-CA-H(–)||SM-CA-O(+); (b) Comparison of cell voltages under 1.0 and 1.5 A cm⁻²; (c) Stability test. Test conditions: 1 M KOH at 60 °C.
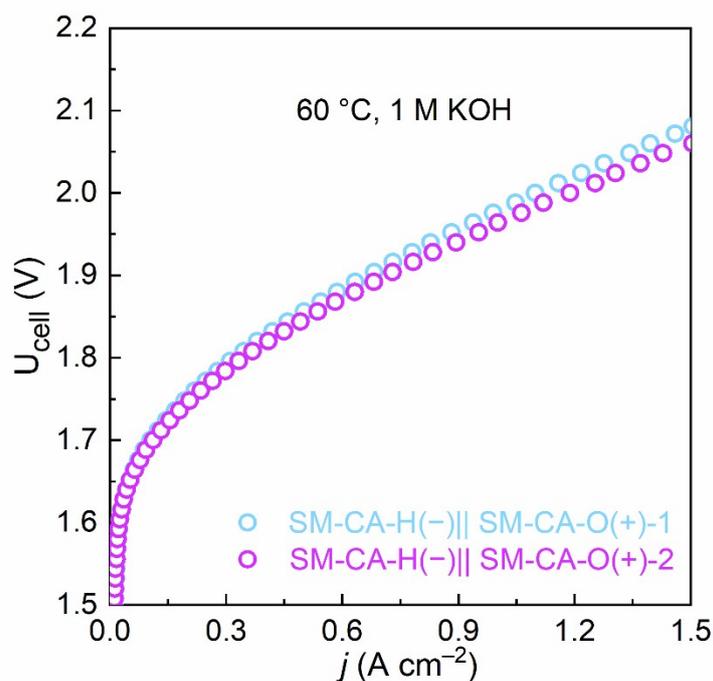
Figure S14. Performance of two modified electrode couples in AEM electrolyzer cell (5 cm^2) at 60 ^{o}C and 1 M KOH.

Table S7. The AEM cell performance of modified electrodes compared with state-of-the-art electrodes reported.

Electrodes/catalysts	Electrodes area (cm^2)	Electrolyte	Temperature (°C)	Cell voltage (V) @ 1 A cm^{-2}	Stability
This work (SM-CA-H(–)‖SM-CA-O(+))	**5**	**1 M KOH**	**25**	**2.33**	**250 h @ 1 A cm^{-2}**
This work (SM-CA-H(–)‖SM-CA-O(+))	**5**	**1 M KOH**	**60**	**1.95**	**120 h @ 1 A cm^{-2}**
NiCoOx catalysts[27]	3.24	1 M KOH	55	2.10	10 h @ 1 A cm^{-2}
NiFeCoOx catalysts[28]	3.24	1 M KOH	70	2.12	-
γ-FeOOH Nanosheet[29]	4	1 M KOH	26	＞2.5	50 h @ 2 V
Pt/C(–)‖Ni foam(+)[30]	5	1 M KOH	80	1.92	-
Pt/C(–)‖Ni felt(+)[31]	5	1 M KOH	60	2.00	20 h @ 2 V
Pt/C(–)‖IrO$_2$(+)[32]	5	1 M KOH	60	1.90	120 h @ 1.8 V
FeCoMnZnMg)$_3$O$_4$[33]	-	1 M KOH	60	1.86	40 h @ 2 V
Ru$_2$P nanofibers[34]	1	1 M KOH	55	1.86	-
Co$_3$S$_4$ nanosheets[35]	-	1 M KOH	45-48	2.20	-
Pt–C core-shell@h-MoS$_2$/GNF[36]	-	1 M KOH	60	2.05	12 h @ 0.5 A cm^{-2}
Co$_3$S$_4$ nanosheet/NF cathode[37]	4.9	1 M KOH	50	2.2	15 h @ 1.85 V
Fe/S-NiOOH//Pt/C[38]	1	1 M KOH	60	2.24	120 h @ 1 A cm^{-2}

Figure S15. The optical image of the 5 cm^2 squared SM-CA-H(−)||SM-CA-O(+) electrodes after 250 h durability test under 1 A cm^{-2}.
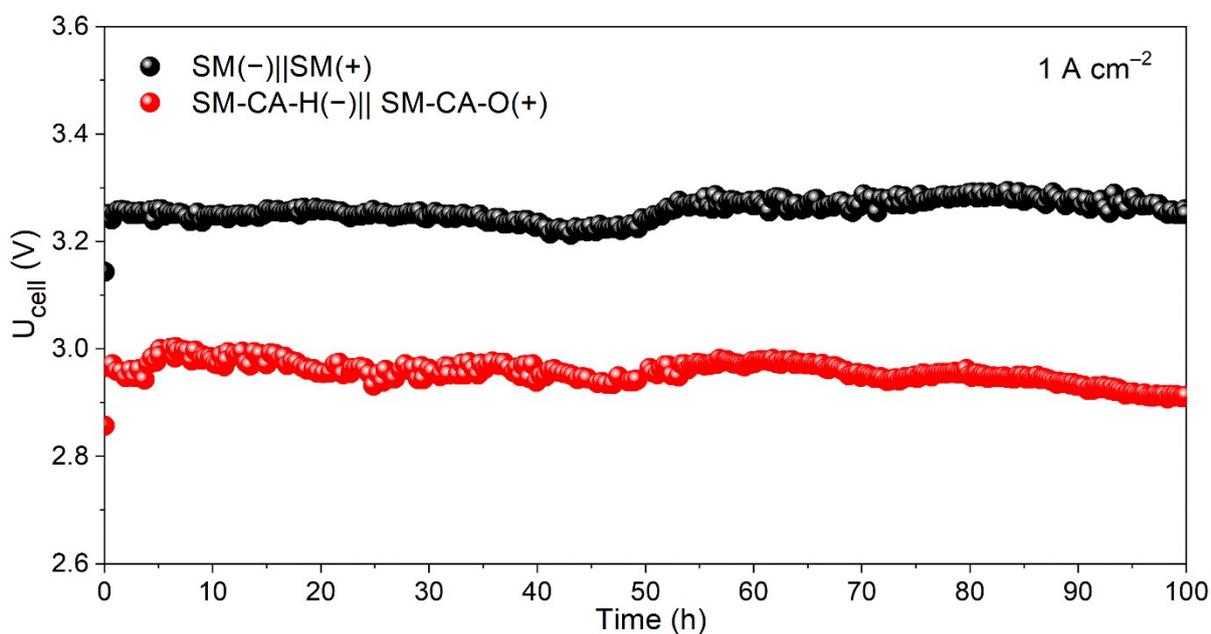

Figure S16. Durability of different alkaline electrolyzer cells (Zirfon PERL as electrode separator): SM(−)||SM(+) and SM-CA-H(−)||SM-CA-O(+).
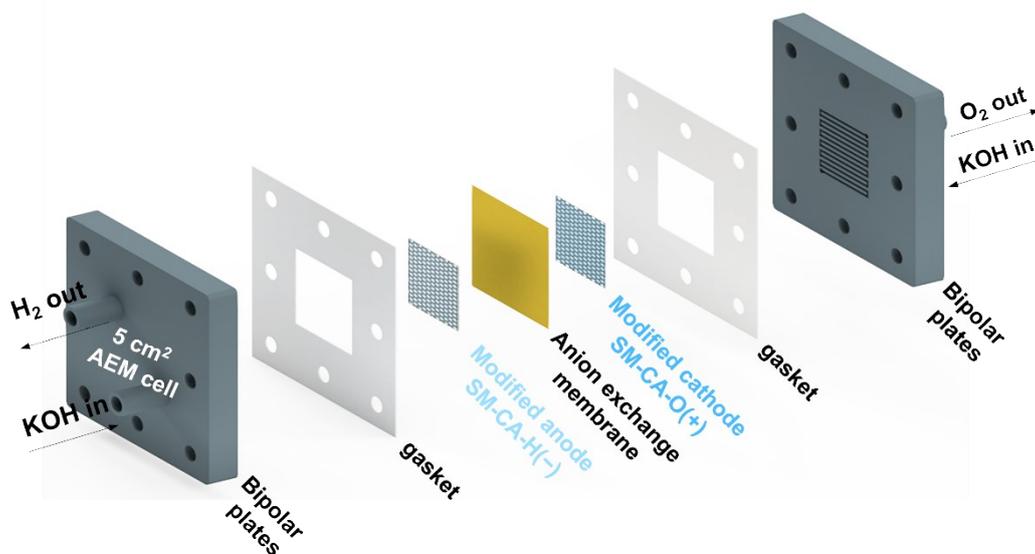
Figure S17. The schematic component of the AEMWE cell.

References

1. H. Chen, J. Li, Y. Shen, W. Jiao, J. Wang, Y. Zou and X. Zou, *Applied Catalysis B: Environmental*, 2022, **316**, 121605.

2. M. S. Balogun, W. Qiu, Y. Huang, H. Yang, R. Xu, W. Zhao, G. R. Li, H. Ji and Y. Tong, *Adv. Mater.*, 2017, **29**, 1702095.

3. W. Hua, H. Sun, M. Jiang, L. Ren, Y. Zhang and J.-G. Wang, *J. Mater. Chem. A*, 2022, **10**, 7366-7372.

4. L. Zhong, L. He, N. Wang, Y. Chen, X. Xie, B. Sun, J. Qian, S. Komarneni and W. Hu, *Applied Catalysis B: Environmental*, 2023, **325**, 122343.

5. Y. Lyu, R. Wang, L. Tao, Y. Zou, H. Zhou, T. Liu, Y. Zhou, J. Huo, S. P. Jiang, J. Zheng and S. Wang, *Appl. Catal. B*, 2019, **248**, 277-285.

6. T. Zhou, H. Gao, Y. Hu, W. Huang, F. Yang, W. Sun and X. Yi, *J. Power Sources*, 2023, **577**, 233241.

7. T. Jiang, X. Jiang, V. Kyriakou, K. Bouzek and H. Liao, *J. Mater. Chem. A*, 2023, **11**, 26011.

8. X. Jiang, V. Kyriakou, B. Wang, S. Deng, S. Costil, C. Chen, T. Liu, C. Deng, H. Liao and T. Jiang, *Chem. Eng. J.*, 2024, **486**, 150180.

9. J. Lee, H. Jung, Y. S. Park, S. Woo, J. Yang, M. J. Jang, J. Jeong, N. Kwon, B. Lim, J. W. Han and S. M. Choi, *Small*, 2021, **17**, e2100639.

10. D. Chanda, K. Kannan, J. Gautam, M. M. Meshesha, S. G. Jang, V. A. Dinh and B. L. Yang, *Applied Catalysis B: Environmental*, 2023, **321**.

11. S. Chen, X. Min, Y. Zhao, X. Wu, D. Zhang, X. Hou, X. Wu, Y. g. Liu, Z. Huang, A. M. Abdelkader, K. Xi and M. Fang, *Advanced Materials Interfaces*, 2022, **9**.

12. S. Garain, C. Dang Van, S. Choi, T. Nguyen Dang, J. W. Ager, K. T. Nam, H. Shin and M. H. Lee, *Advanced Materials Interfaces*, 2022, **9**.

13. M. M. Hasan, A. K. Gomaa, G. E. Khedr, K. E. Salem, B. S. Shaheen and N. K. Allam, *Energy & Fuels*, 2022, **36**, 14371-14381.

14. L. Jia, G. Du, D. Han, Y. Wang, W. Zhao, Q. Su, S. Ding and B. Xu, *Chem. Eng. J.*, 2023, **454**.

15. A. Saad, Y. Gao, K. A. Owusu, W. Liu, Y. Wu, A. Ramiere, H. Guo, P. Tsiakaras and X. Cai, *Small*, 2022, **18**, e2104303.

16. J. Shen, Q. Li, W. Zhang, Z. Cai, L. Cui, X. Liu and J. Liu, *J. Mater. Chem. A*, 2022, **10**, 5442-5451.

17. G. Song, S. Luo, Q. Zhou, J. Zou, Y. Lin, L. Wang, G. Li, A. Meng and Z. Li, *J. Mater. Chem. A*, 2022, **10**, 18877-18888.

18. Y. Zhang, S. Chen, Y. Zhang, R. Li, B. Zhao and T. Peng, *Adv. Mater.*, 2023, **35**, e2210727.

19. G. Bahuguna, A. Cohen, N. Harpak, B. Filanovsky and F. Patolsky, *Small Methods*, 2022, **6**, e2200181.

20. Z. He, Y. He, Y. Qiu, Q. Zhao, Z. Wang, X. Kang, L. Yu, L. Wu and Y. Jiang, *Applied Catalysis B: Environmental*, 2024, **342**.

21. A. Li, L. Zhang, F. Wang, L. Zhang, L. Li, H. Chen and Z. Wei, *Applied Catalysis B: Environmental*, 2022, **310**.

22. W. Luo, Y. Wang, L. Luo, S. Gong, M. Wei, Y. Li, X. Gan, Y. Zhao, Z. Zhu and Z. Li, *ACS Catalysis*, 2022, **12**, 1167-1179.

23. Q. lv, B. Yao, W. Zhang, L. She, W. Ren, L. Hou, Y. Fautrelle, X. Lu, X. Yu and X. Li, *Chem. Eng. J.*, 2022, **446**.

24. Y. Wang, B. Liu, X. Shen, H. Arandiyan, T. Zhao, Y. Li and C. Zhao, *Adv. Energy Mater.*, 2021, **11**, 2003759.

25. Z. Zang, Q. Guo, X. Li, Y. Cheng, L. Li, X. Yu, Z. Lu, X. Yang, X. Zhang and H. Liu, *J. Mater. Chem. A*, 2023, **11**, 4661-4671.

26. X. Zhao, X. Yong, Q. Ji, Z. Yang, Y. Song, Y. Sun, Z. Cai, J. Xu, L. Li, S. Shi, F. Chen, C. Li, P. Wang and J.-B. Baek, *J. Mater. Chem. A*, 2023, **11**, 12726-12734.

27. K. W. Ahmed, S. Habibpour, Z. Chen and M. Fowler, *Journal of Energy Storage*, 2024, **79**.

28. K. W. Ahmed, M. J. Jang, S. Habibpour, Z. Chen and M. Fowler, *Electrochem*, 2022, **3**, 843-861.

29. D. K. Bora, D. Ghosh, A. Jana, R. K. Nagarale and A. B. Panda, *ACS Applied Engineering Materials*, 2024, **2**, 975-987.

30. T. Caielli, A. R. Ferrari, S. Bonizzoni, E. Sediva, A. Caprì, M. Santoro, I. Gatto, V. Baglio and P. Mustarelli, *J. Power Sources*, 2023, **557**.

31. N. Carboni, L. Mazzapioda, A. Caprì, I. Gatto, A. Carbone, V. Baglio and M. A. Navarra, *Electrochim. Acta*, 2024, **486**.

32. I. Gatto, A. Caprì, C. Lo Vecchio, S. Zignani, A. Patti and V. Baglio, *Int. J. Hydrogen Energy*, 2023, **48**, 11914-11921.

33. S. C. Karthikeyan, S. Ramakrishnan, S. Prabhakaran, M. R. Subramaniam, M. Mamlouk, D. H. Kim and D. J. Yoo, *Small*, 2024, DOI: 10.1002/smll.202402241, e2402241.

34. J.-C. Kim, J. Kim, J. C. Park, S. H. Ahn and D.-W. Kim, *Chem. Eng. J.*, 2021, **420**.

35. Y. S. Park, J. H. Lee, M. J. Jang, J. Jeong, S. M. Park, W.-S. Choi, Y. Kim, J. Yang and S. M. Choi, *Int. J. Hydrogen Energy*, 2020, **45**, 36-45.

36. S. Ramakrishnan, S. Vijayapradeep, S. C. Selvaraj, J. Huang, S. C. Karthikeyan, R. Gutru, N. Logeshwaran, T. Miyazaki, M. Mamlouk and D. J. Yoo, *Carbon*, 2024, **220**.

37. X. She, C. Feng, D. Liu, Z. Fan, M. Yang and Y. Li, *Int. J. Hydrogen Energy*, 2024, **59**, 1297-1304.

38. F. L. Wang, J. L. Tan, Z. Y. Jin, C. Y. Gu, Q. X. Lv, Y. W. Dong, R. Q. Lv, B. Dong and Y. M. Chai, *Small*, 2024, **20**, e2310064.